

Edge-Preserving Image Decomposition using L1 Fidelity with L0 Gradient

Chih-Tsung Shen*
National Taiwan University

Feng-Ju Chang†
Academia Sinica

Yi-Ping Hung‡
National Taiwan University

Soo-Chang Pei§
National Taiwan University

Abstract

We present an image decomposition method using L1 fidelity term with L0 norm of gradient to decompose an image into base layer and detail layer. Generally, the L1 fidelity should be preferable to the L2 norm when the erroneous measurements exist. It is also reported that the L0 norm of gradient is a better prior term than total variation and the L2 norm of gradient. Therefore, we combine these two benefits to obtain our base layer by adopting our method using L1 fidelity and L0 gradient. Our image decomposition method can be regarded as the fundamental tool to generate multiple image editing applications, such as image denoising, edge detection, detail enhancement, cartoon JPEG artifact removal, local tone mapping, and contrast enhancement under low backlight condition. Experimental results show that our proposed method is promising as compared to the existing methods.

CR Categories: I.3.3 [Computer Graphics]: Picture/Image Generation—Display Algorithms I.4.3 [Image Processing and Computer Vision]: Enhancement—Filtering; I.4.3 [Image Processing and Computer Vision]: Enhancement—Smoothing;

Keywords: image decomposition, L1 Fidelity, L0 Sparsity,

1 Introduction

Image decomposition refers to decompose the image signal into several layer signals: base layer and detail layer. In order to avoid the signal reversal and the Halo artifact around edges, the edge-preserving base layer is usually required. With these decomposed signals, we can not merely obtain more flexibility to adjust each signal but also develop plenty of image editing applications, such as image smoothing [Tomasi and Manduchi 1998] [Subr et al. 2009] [He et al. 2010] [Xu et al. 2011], HDR imaging [Durand and Dorsey 2002] [Meylan and Susstrunk 2006] [Chen et al. 2007], image abstraction/stylization [Winnemoller et al. 2006] [Farbman et al. 2008], and image fusion [Fattal et al. 2007]. Due to the wide variety of interesting applications, image decomposition becomes an important technique in the related field of computer vision, computer graphics and computational photography.

In 1998, Tomasi et al. obtained their base layer by simultaneously

*e-mail:shenchihtsung@gmail.com

†e-mail:fengju514@gmail.com

‡e-mail:hung@csie.ntu.edu.tw

§e-mail:pei@cc.ee.ntu.edu.tw

Copyright © 2012 by the Association for Computing Machinery, Inc.

Permission to make digital or hard copies of part or all of this work for personal or classroom use is granted without fee provided that copies are not made or distributed for commercial advantage and that copies bear this notice and the full citation on the first page. Copyrights for components of this work owned by others than ACM must be honored. Abstracting with credit is permitted. To copy otherwise, to republish, to post on servers, or to redistribute to lists, requires prior specific permission and/or a fee. Request permissions from Permissions Dept, ACM Inc., fax +1 (212) 869-0481 or e-mail permissions@acm.org.

SIGGRAPH Asia 2012, Singapore, November 28 – December 1, 2012.

© 2012 ACM 978-1-4503-1757-3/12/0011\$15.00

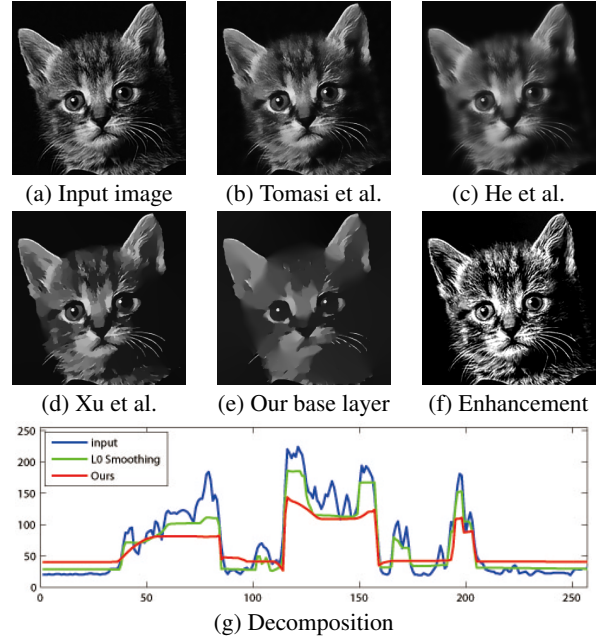


Figure 1: Base layer images and the 1D-result. The blue line is the 150-th row of the input image, and the green line is the 150-th row of the Xu et al.'s L0 smoothing result. The red line is the 150-th row of our image decomposition using L1 fidelity and L0 gradient.

filtering both position and the gray-level value of the position. Their bilateral filtering inspires researchers to develop the edge-aware processing while branches out thousands of interesting applications [Tomasi and Manduchi 1998]. Durand et al. and Chen et al. proposed their linear approximations to speed up Tomasi et al.'s bilateral filtering by using Fast Fourier Transformations and grid structure, respectively [Durand and Dorsey 2002] [Chen et al. 2007]. Lately, Farbman et al. proposed their edge-preserving decompositions for multi-scale tone and detail manipulation [Farbman et al. 2008]. He et al. also proposed their guided filter for processing [He et al. 2010]. Gastal et al. smoothed the signals in their specified domain. Afterwards, they transformed the smooth versions back to the original domain so as to complete their edge-aware image and video editing [Gastal and Oliveira 2011].

In this technical brief, we present a new edge-preserving image decomposition model. Different to the previous works to adopt the L2 fidelity term, we adopt the L1 fidelity term. Based on the perspective of compressive sensing, Yang et al. reported that L1 fidelity is generally better than L2 fidelity when erroneous measurements exist [Yang and Zhang 2009]. In addition, Xu et al. examined the different priors and also demonstrated that L0 norm of gradient is better than total variation and weighted L2 norm of gradient [Xu et al. 2011]. We combine these two beneficial parts and propose our image decomposition using L1 fidelity term with L0 norm of gradient to generate the edge-preserving base layer and its corresponding detail layer. In our knowledge, we are the first to deal with the minimization using L1 fidelity with L0 gradient.

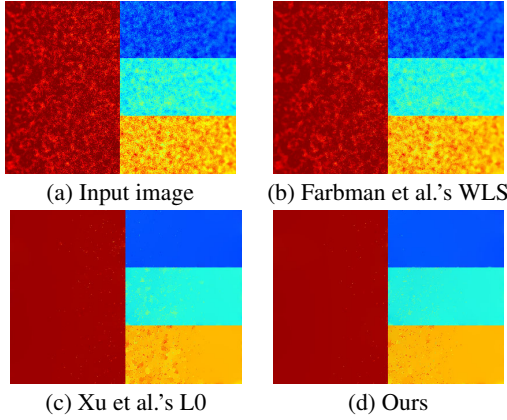


Figure 2: Image denoising. We adopt the same balancing parameter $\lambda = 0.1$ to remove the noise. As we can see that our model outperforms the compared methods.

2 Model for L1 Fidelity with L0 Gradient

Let $L(x, y)$ be the input observation, $B(x, y)$ represent the base layer image, and $D(x, y)$ be the detail layer image. We can model our image decomposition as the following relationship:

$$L(x, y) = B(x, y) + D(x, y) \quad (1)$$

However, it is an ill-posed problem to decompose one image into two images. Therefore, we construct the minimization with the constraints on edges to pursuit the resulting base layer. It is reported that L1 fidelity term is better than L2 fidelity term when erroneous measurements exist [Yang and Zhang 2009]. We adopt L1 fidelity to calculate the difference between the base layer and the input observation. Generally, the L0-norm of gradient represents the numbers of non-zero gradient. Adopting the L0-norm of gradient can force the minimization to generate the base layer which is close to the original signal when meeting strong edges. With the definition above, the base layer $B(x, y)$ can be estimated by solving

$$\min_{B(x, y)} \sum_{(x, y)} |B(x, y) - L(x, y)| + \lambda \cdot C(B(x, y)) \quad (2)$$

where $C(B(x, y))$ represents the regularization term. Since we adopt the L0-norm of gradient, $C(B(x, y))$ represents the numbers of non-zero gradient and can be expressed as $C(B(x, y)) = \#\{(x, y) | |\nabla B(x, y)| \neq 0\}$, where $\#$ denotes the numbers of pixels while ∇ denotes the difference operator.

3 Solver for L1 Fidelity with L0 Gradient

We can easily figure out that (2) contains non-linear penalties for both fidelity term and regularization term. We base on the half-quadratic splitting and approximation for L1 minimization to solve (2) by using an efficient alternating minimization method [Wang et al. 2008] [Xu and Jia 2010]. To solve the L1 fidelity, we introduce an auxiliary variable $w(x, y)$ to replace the difference between $B(x, y)$ and $L(x, y)$. Besides, the difference between $(B(x, y) - L(x, y))$ and $w(x, y)$ is also penalized as a quadratic term, yielding the following approximation model to (2):

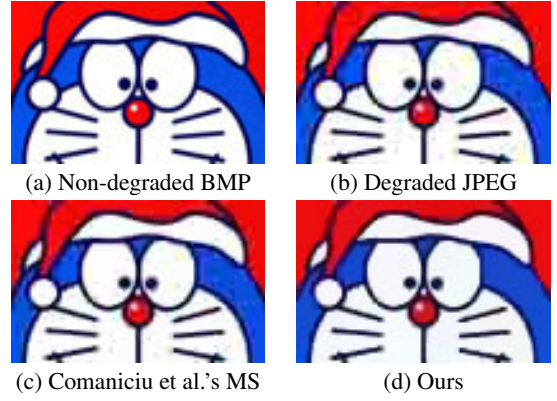


Figure 3: JPEG artifact removal. Please notice the regions in blue. We remove the compression artifact successfully as compared to Comaniciu et al.'s mean shift.

$$\begin{aligned} & \min_{B, w, a_x, a_y} \alpha \cdot \sum_{(x, y)} |B(x, y) - L(x, y) - w(x, y)|^2 + \sum_{(x, y)} |w(x, y)| \\ & + \lambda \cdot (\#\{(x, y) | \frac{\partial B(x, y)}{\partial x} + \frac{\partial B(x, y)}{\partial y} \neq 0\}) \end{aligned} \quad (3)$$

To solve the L0 norm of gradient, we introduce another two auxiliary variables $a_x(x, y)$ and $a_y(x, y)$ to replace the gradient $\frac{\partial B(x, y)}{\partial x}$ in x-direction and the gradient $\frac{\partial B(x, y)}{\partial y}$ in y-direction, respectively. Then, we reconstruct our minimization as

$$\begin{aligned} & \min_{B, w, a_x, a_y} \alpha \cdot \sum_{(x, y)} |B(x, y) - L(x, y) - w(x, y)|^2 \\ & + \sum_{(x, y)} |w(x, y)| + \lambda \cdot C(a_x(x, y), a_y(x, y)) \\ & + \beta \cdot (|\frac{\partial B(x, y)}{\partial x} - a_x(x, y)|^2 + |\frac{\partial B(x, y)}{\partial y} - a_y(x, y)|^2) \end{aligned} \quad (4)$$

where $C(a_x(x, y), a_y(x, y)) = \#\{(x, y) | |a_x(x, y)| + |a_y(x, y)| \neq 0\}$ and β is the automatic tuning parameter.

3.1 Solver: Computing $\mathbf{B}(x, y)$

To solve (4), we adopt the alternating minimization (AM) algorithm to fix one set of variables while obtain another set of variables. We can fix $w(x, y)$, $a_x(x, y)$ and $a_y(x, y)$ to simplify (4) and obtain the $B(x, y)$ by solving the following minimization:

$$\begin{aligned} & \min_B \frac{\alpha}{\beta} \cdot \sum_{(x, y)} |B(x, y) - L(x, y) - w(x, y)|^2 \\ & + |\frac{\partial B(x, y)}{\partial x} - a_x(x, y)|^2 + |\frac{\partial B(x, y)}{\partial y} - a_y(x, y)|^2 \end{aligned} \quad (5)$$

Using the convolution theorem of Fourier Transformations and diagonalized derivative operators, we can solve (5) by using the Fast Fourier Transformations and also speed up the whole process.

$$\begin{aligned} & B(x, y) = \\ & F^{-1} \left\{ \frac{\alpha F(L) + \alpha F(w) + \beta F^*(\partial x)F(a_x) + \beta F^*(\partial y)F(a_y)}{\alpha + \beta F^*(\partial x)F(\partial x) + \beta F^*(\partial y)F(\partial y)} \right\} \end{aligned} \quad (6)$$

where “ $*$ ” denotes complex conjugacy, the multiplication is componentwise, and the division is also componentwise.

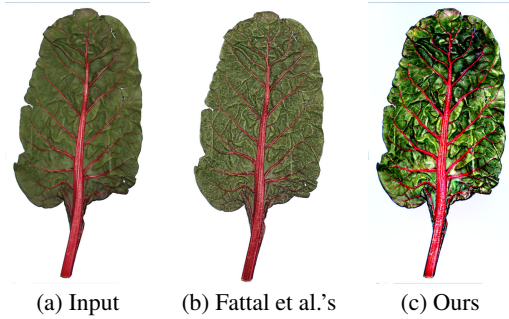


Figure 4: Detail enhancement.

3.2 Solver: Computing auxiliary variables

In the next iteration, we fix the estimated $B(x, y)$ to obtain the new $w(x, y)$, $a_x(x, y)$ and $a_y(x, y)$. Since $w(x, y)$ is independent to $a_x(x, y)$ and $a_y(x, y)$, we can solve $w(x, y)$ by solving the following minimization, which is extracted from (4).

$$\min_{w(x, y)} |w(x, y)| + \alpha \cdot |B(x, y) - L(x, y) - w(x, y)|^2 \quad (7)$$

for which the unique solver is given using matrix calculus, and we can generate the solution by the following expression:

$$w(x, y) = \max\{|B(x, y) - L(x, y)| - \frac{1}{2\alpha}, 0\} \frac{B(x, y) - L(x, y)}{|B(x, y) - L(x, y)|} \quad (8)$$

where the fraction represents the sign function, α is the parameter which we set to 1, and we also have the convention $0 \cdot (0/0) = 0$.

In addition, we can also solve $a_x(x, y)$ and $a_y(x, y)$ by solving the following minimization, which is also extracted from (4).

$$\begin{aligned} & \min_{a_x, a_y} \frac{\lambda}{\beta} \cdot C(a_x(x, y), a_y(x, y)) \\ & + |\frac{\partial B(x, y)}{\partial x} - a_x(x, y)|^2 + |\frac{\partial B(x, y)}{\partial y} - a_y(x, y)|^2 \end{aligned} \quad (9)$$

where the L0-norm of gradient can be modeled as:

$$C(a_x(x, y), a_y(x, y)) = H(|a_x(x, y)| + |a_y(x, y)|) \quad (10)$$

where $H(|a_x(x, y)| + |a_y(x, y)|)$ is a binary function returning 1 when $|a_x(x, y)| + |a_y(x, y)| \neq 0$ and returning 0 otherwise.

By alternatively calculating the minimizations in (6), (8) and (9), we can obtain our final base layer $\hat{B}(x, y)$

3.3 Detail Layer and Enhancement

Since we obtain $\hat{B}(x, y)$, we can also obtain our corresponding detail layer $\hat{D}(x, y)$.

$$\hat{D}(x, y) = L(x, y) - \hat{B}(x, y) \quad (11)$$

With the estimated base layer and its corresponding detail layer, we can generate plenty of image editing applications. In the general form, we can enhance the input image by correcting the base layer and boosting the detail layer.

$$L_{EN}(x, y) = s \cdot W \cdot (\frac{\hat{B}(x, y)}{W})^\gamma + G \cdot \hat{D}(x, y) \quad (12)$$

where s is a scale parameter, W is the white value (equal to 1 in normalized images or 255 for 8-bits images), γ is the parameter for gamma correction, and G is the gain for detail boosting.

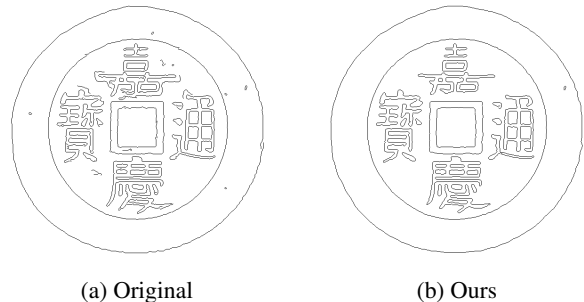
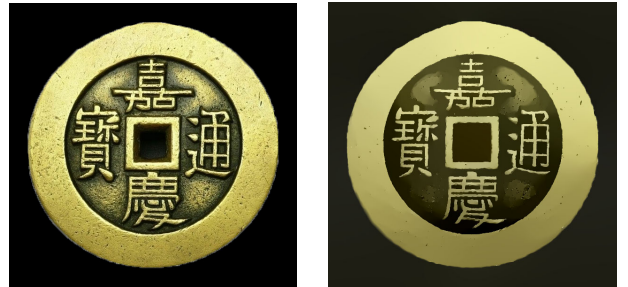


Figure 5: Edge detection. Our method can be the pre-processing filter to remove the noise before detecting the edges.

4 Applications

4.1 Image Smoothing, Denoising and Artifact Removal

First, we demonstrate our image smoothing and enhancement with $\lambda = 0.01$ in Fig. 1. We decompose the input image into base layer and detail layer. We can obtain the image smoothing result by using only the base layer. We can also enhance the image using (11) with $s = 1$, $\gamma = 1$, and $G = 3$. Fig. 1(g) is the 1-D decomposition result. The blue line is the 150-th row of input image. The green line is the base layer of Xu et al.’s L0 smoothing. The red line is our base layer. As we can see that the L1 fidelity term gives the wild smooth result while the L0 gradient prior preserves edges successfully. In Fig. 2, we obtain our base layer so as to denoise an image. We also examine the power of the L1 fidelity as compared to Farbman et al.’s weighted least-square (WLS) method [Farbman et al. 2008] and Xu et al.’s L0 smoothing [Xu et al. 2011]. Using the same balancing parameter $\lambda = 0.1$, we can obtain the better result. Please notice the regions near the red-yellow junctions. In Fig. 3, we adopt our image decomposition to remove the cartoon JPEG artifact by using our base layer. As compared to Comaniciu et al.’s mean shift [Comaniciu and Meer 2002], we can almost obtain an artifact-free result. Please notice the regions in blue in Fig. 3. It is corrupted in Fig. 3(b) and Fig. 3(c), but not in Fig. 3(d).

4.2 Edge Detection and Detail Enhancement

In addition, we can also only enhance our detail layer with $\lambda = 0.01$ and $G = 5$. In Fig. 4, we use only one input image and outperforms the Fattal et al.’s multiple-images scheme in global contrast and local information [Fattal et al. 2007]. Besides, our method can be a pre-processing method for the traditional image processing applications. For edge detection, we can pre-filter the input image to remove the noise and then detect the edges. We adopt $\lambda = 0.05$ for our decomposition. In Fig. 5, we can see that our detected edges is more correct than the comparison.

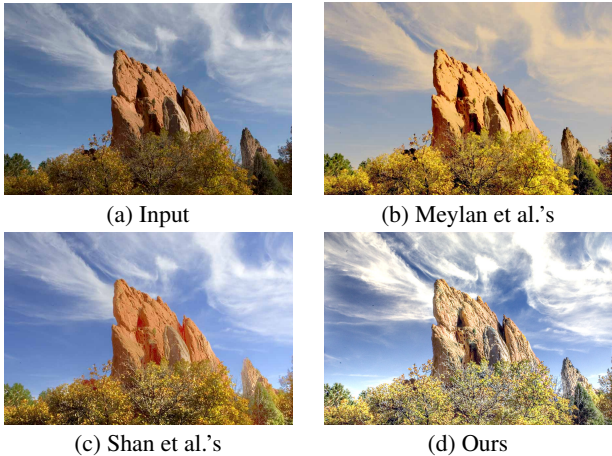


Figure 6: Local tone mapping. Our image decomposition can adjust the base layer for global view and enhance the detail for local view. Different to Meylan et al.’s to enhance in PCA color space, we only process our decomposition on V-channel of HSV color space.

4.3 Tone-Mapping and Backlight

Our image decomposition is also useful for rendering images on displays. Our method also benefit the local tone mapping technique. We adopt $\lambda = 0.01$, $s = 1$, $\gamma = 2.2$, and $G = 3$ to enhance the V-channel of input image in HSV color space. Fig. 6(b) is Meylan et al.’s tone mapping result [Meylan and Susstrunk 2006], and Fig. 6(c) is Shan et al.’s result [Shan et al. 2010]. Our tone-mapping result is shown in Fig. 6(d). In addition, our method can also be the fundamental base to adjust both global brightness and local detail on backlight-scaled displays. Once using 40% backlight, it can save almost 90% power of the displays. Fig. 7(a) is the input image using full 100% backlight. Fig. 7(b) is the simulated image which is linear-scaled to 40% in the V-channel. It can be used to simulate the visual quality of input image using only 40% backlight. Fig. 7(c) is simulated result of Durand et al.’s method under 40% backlight [Durand and Dorsey 2002]. Fig. 7(d) is our simulated result using the parameters $s = 0.4$, $\gamma = 2.2$ and $G = 2$. As we can see our simulated result is better in global contrast.

5 Conclusions

In this paper, we present the minimization using L1 data term with L0 gradient. Based on compressive sensing, L1 fidelity term is better than L2 fidelity term when the erroneous measurements exist. Besides, it is also reported that the L0 gradient is a better prior term than total variation and the weighted L2 gradient. We combine these two benefits and construct our image decomposition method. Using our base layer and detail layer, we generate plenty of image editing applications. Experimental results show that our proposed method is promising as compared to the existing methods.

References

- CHEN, J., PARIS, S., AND DURAND, F. 2007. Real-time edge-aware image processing with the bilateral grid. In *Proceedings of SIGGRAPH*, no. 103.
- COMANICIU, D., AND MEER, P. 2002. Mean shift: a robust approach toward feature space analysis. *IEEE Transactions on Pattern Analysis and Machine Intelligence* 24, 5 (May), 603–619.
- DURAND, F., AND DORSEY, J. 2002. Fast bilateral filtering for the display of high-dynamic range images. In *Proceedings of SIGGRAPH*, 257–266.
- FARMBMAN, Z., FATTAL, R., LISCHINSKI, D., AND SZELISKI, R. 2008. Edge-preserving decompositions for multi-scale tone and detail manipulation. In *Proceedings of SIGGRAPH*, 671–680.
- FATTAL, R., AGRAWALA, M., AND RUSINKIEWICZ, S. 2007. Multiscale shape and detail enhancement from multi-light image collections. In *Proceedings of SIGGRAPH*, no. 51.
- GASTAL, E., AND OLIVEIRA, M. 2011. Domain transform for edge-aware image and video processing. In *Proceedings of SIGGRAPH*, no. 33.
- HE, K., SUN, J., AND TANG, X. 2010. Guided image filtering. In *Proceedings of ECCV*, 15–22.
- MEYLAN, M., AND SUSSTRUNK, S. 2006. High dynamic range image rendering with a retinex-based adaptive filter. *IEEE Transactions on Image Processing* 15, 9 (September), 2820–2830.
- SHAN, Q., JIAYA, J., AND BROWN, M. 2010. Globally optimized linear windowed tone-mapping. *IEEE Transactions on Visualization and Computer Graphics* 16, 4 (July), 663–675.
- SUBR, K., SOLER, C., AND DURAND, F. 2009. Edge-preserving multiscale image decomposition based on local extrema. In *Proceedings of SIGGRAPH ASIA*, no. 147.
- TOMASI, C., AND MANDUCHI, R. 1998. Bilateral filtering for gray and color images. In *Proceedings of ICCV*, 836–846.
- WANG, Y., J. YANG, W. Y., AND ZHAN, Y. 2008. A new alternating minimization algorithm for total variation image reconstruction. *SIAM Journal on Imaging Sciences* 1, 3, 248–272.
- WINNEMOLLER, H., OLSEN, S. C., AND GOOCH, B. 2006. Real-time video abstraction. In *Proceedings of SIGGRAPH*, 1221–1226.
- XU, L., AND JIA, J. 2010. Two-phase kernel estimation for robust motion deblurring. In *Proceedings of ECCV*, 157–170.
- XU, L., LU, C., XU, Y., AND JIA, J. 2011. Image smoothing via l_0 gradient minimization. In *Proceedings of SIGGRAPH ASIA*, no. 174.
- YANG, J., AND ZHANG, Y. 2009. Alternating direction algorithms for l_1 -problems in compressive sensing. *CAAM TR09-37*.

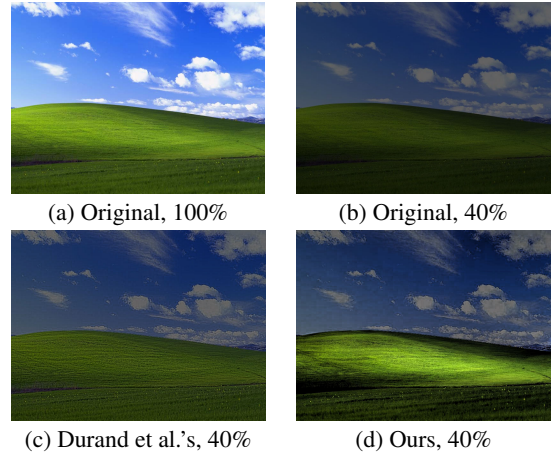


Figure 7: Image Enhancement under Low Backlight.